

# Imprints of the Janis-Newman-Winicour spacetime on observations related to shadow and accretion

Subhadip Sau\*, Indrani Banerjee† and Soumitra SenGupta‡

School of Physical Sciences, Indian Association for the Cultivation of Science, Kolkata-700032, India

## Abstract

The final fate of gravitational collapse of massive stars has been a subject of interest for a long time since such a collapse may lead to black holes and naked singularities alike. Since, the formation of naked singularities is forbidden by the cosmic censorship conjecture, exploring their observational differences from black holes may be a possible avenue to search for these exotic objects. The simplest possible naked singularity spacetime emerges from the Einstein massless scalar field theory with the advantage that it smoothly translates to the Schwarzschild solution by the variation of the scalar charge. This background, known as the Janis-Newman-Winicour spacetime is the subject of interest in this work. We explore electromagnetic observations around this metric which involves investigating the characteristics of black hole accretion and shadow. We compute the shadow radius in this spacetime and compare it with the image of M87\*, recently released by the Event Horizon Telescope Collaboration. Similarly, we derive the expression for the luminosity from the accretion disk and compare it with the observed optical luminosity of eighty Palomar Green quasars. Our analysis indicates that the shadow of M87\* favors the Schwarzschild background while the quasars on the other hand exhibit the existence of a non-trivial scalar charge from the accretion data thereby supporting the Janis-Newman-Winicour spacetime. The implications of this result are discussed.

## 1 Introduction

One of the classic unresolved problems in general relativity is the ultimate fate of the gravitational collapse of a massive body, such as a star. It has been conjectured that the end state of any generic complete gravitational collapse leads to a Kerr black hole characterized by only its mass and angular momentum. All other information regarding the initial conditions of the collapse, the symmetries and the nature of matter fields that were present in the beginning of the collapse gets radiated away. It turns out that it is very difficult to prove this conjecture either analytically or numerically and therefore one cannot definitively say that the ultimate fate of a gravitational collapse always leads to the formation of a black hole. In fact, investigations reveal that such gravitational collapse with a set of allowed initial conditions often lead to the formation of naked singularities [1–11], even though such objects are forbidden by the cosmic censorship conjecture [12].

While the end products of gravitational collapse continues to be debatable, it is worth exploring the observational differences between black holes and naked singularities, assuming that they have been formed

---

\*tpss2@iacs.res.in

†tpib@iacs.res.in

‡tpssg@iacs.res.in

by some mechanism. Given the surfeit of data available in the electromagnetic domain, this has intrigued researchers worldwide since such a study can enhance our understanding regarding the nature of compact objects at the galactic centres or in the X-ray binaries. Observations related to accretion disks [13–19] or gravitational lensing [20–26] have revealed that black holes and naked singularities often exhibit strikingly different properties which can be used as a possible probe to differentiate between them. Further, ultra high energy collisions and fluxes of the escaping collision products can be another possible tool to discern between the two different entities [27]. There are however cases when certain wormhole spacetimes and naked singularities exhibit similar observational features like that of a black hole which makes the differentiation quite difficult [28–31]. However, this will be kept outside the purview of the present discussion.

In the present work we consider the Janis-Newman-Winicour (JNW) naked singularity which represents an exact solution of the Einstein’s equations with a massless scalar field [32]. This solution was originally derived by Fisher [33] in a different parametrization while Bronnikov & Khodunov [34] subsequently studied its stability. It was later rediscovered by Wyman [35] and the equivalence of the Wyman solution with the Janis-Newman-Winicour spacetime was established by Virbhadra [36]. It is interesting to note that addition of the massless scalar field in the action changes the nature of the spherically symmetric and asymptotically flat exact metric solution from the Schwarzschild black hole to the JNW naked singularity. Consequently, it can be shown that one can recover the Schwarzschild metric from the JNW spacetime by continuously adjusting a single metric parameter representative of the scalar charge of the naked singularity.

There exists several works in the literature which explored the optical properties of the Janis-Newman-Winicour spacetime, e.g. gravitational lensing and relativistic images [23–26, 37], accretion and shadow [21, 22, 37, 38]. The aim of this work is to explore the nature of shadow and the emission from the accretion disk around the Janis-Newman-Winicour spacetime and compare them with the available observations. The optical luminosity of eighty Palomar Green quasars and the recently released shadow of M87\* are used as the observational sample for comparing the theoretical results.

The paper is organized as follows: In Section 2 we review the basic properties of the Janis-Newman-Winicour spacetime. We study the structure of the shadow cast by the JNW spacetime and compare it with the image of M87\* in Section 3. Section 4 serves as a quick overview over the ‘thin accretion disk’ model proposed by Novikov & Thorne which helps us to evaluate the accretion disk luminosity for a sample of eighty Palomar Green quasars. Subsequently we compare this with the observed luminosity of the quasars to distinguish the JNW spacetime from the Schwarzschild background. We end with a summary of our results and the concluding remarks in Section 5.

We use  $(-, +, +, +)$  as the metric convention and will work with geometrized units taking  $G = c = 1$ .

## 2 Janis-Newman-Winicour spacetime: A quick review

In this work we consider the Einstein massless scalar (EMS) field theory such that the massless scalar field is minimally coupled to gravity. The associated action is given by

$$ds^2 = \int d^4x \sqrt{-g} \left[ \frac{R}{2\kappa^2} - \frac{1}{2} \partial_\mu \phi(r) \partial^\mu \phi(r) \right] \quad (1)$$

where,  $g$  and  $R$  are respectively, determinant of the metric tensor and the Ricci scalar,  $\kappa^2 = 8\pi G$  ( $G$  is the four-dimensional gravitational constant) and  $\phi(r)$  is the minimally coupled scalar field. In four dimension, the corresponding Einstein’s gravitational field equations derived from the above action has an exact static

and spherically symmetric solution [36, 39, 40] given by,

$$ds^2 = - \left(1 - \frac{b}{\tilde{r}}\right)^\gamma dt^2 + \left(1 - \frac{b}{\tilde{r}}\right)^{-\gamma} dr^2 + \left(1 - \frac{b}{\tilde{r}}\right)^{1-\gamma} r^2 (d\theta^2 + \sin^2 \theta d\phi^2) \quad (2)$$

which is popularly known as the Janis-Newman-Winicour solution in the literature. In Eq. (2)  $0 \leq \gamma \leq 1$ ,  $\tilde{r} = rc^2/GM$  and  $b\gamma = 2$ , such that the Schwarzschild metric is retrieved when  $\gamma = 1$ . There is a curvature singularity at  $\tilde{r} = b$  which is also the location of the event horizon. Since the singularity is not cloaked by the event horizon this metric represents a naked singularity and hence we confine ourselves in the region  $\tilde{r} > b$ . The solution for the scalar field and the associated energy-momentum tensor are respectively given by

$$\phi(r) = \frac{q}{b} \ln \left(1 - \frac{b}{\tilde{r}}\right) \quad \text{and} \quad (3)$$

$$T_{\mu\nu} = \partial_\mu \phi \partial_\nu \phi - \frac{1}{2} g_{\mu\nu} \partial^\alpha \phi \partial_\alpha \phi \quad (4)$$

where  $b$  is related to the scalar charge  $q$  by,

$$b = 2\sqrt{1 + q^2} \quad (5)$$

such that smaller  $\gamma$  corresponds to a larger magnitude of the scalar field.

In the context of string theory a pseudo scalar field known as the axion, arises as the dual of the field strength of the Kalb-Ramond field  $B_{\mu\nu}$  minimally coupled to Einstein gravity in four dimensions. The Kalb-Ramond field  $B_{\mu\nu}$  with the transformation property of a second rank anti-symmetric tensor gauge field has the following action,

$$S_{KR} = \int d^4x \sqrt{-g} \left[ \frac{R}{2\kappa^2} - \frac{1}{12} H_{\mu\nu\alpha} H^{\mu\nu\alpha} \right] \quad (6)$$

where  $H_{\alpha\mu\nu} = \partial_{[\alpha} B_{\mu\nu]}$  is the field strength tensor which has the pseudo-scalar axion field  $H$  as its dual,

$$H^{\alpha\mu\nu} = \epsilon^{\alpha\mu\nu\beta} \partial_\beta H \quad (7)$$

In terms of the axion field the energy-momentum tensor of the Kalb-Ramond field can be written as

$$T_{\mu\nu} = \partial_\mu H \partial_\nu H - \frac{1}{2} g_{\mu\nu} \partial^\sigma H \partial_\sigma H \quad (8)$$

which resembles Eq. (4).

Under a different choice of the metric ansatz, the resultant static, spherically symmetric and asymptotically flat solution of the Einstein's equations (associated with the Kalb-Ramond field) assumes a perturbative solution of the the form [41],

$$ds^2 = -e^{\nu(\tilde{r})} dt^2 + e^{\lambda(\tilde{r})} dr^2 + r^2 d\Omega^2 \quad (9)$$

such that

$$e^{\nu(\tilde{r})} = 1 - \frac{2}{\tilde{r}} + \frac{h}{\tilde{r}^3} + \mathcal{O}\left(\frac{1}{\tilde{r}^4}\right) \quad (10a)$$

$$e^{-\lambda(\tilde{r})} = 1 - \frac{2}{\tilde{r}} + \frac{3h}{\tilde{r}^2} + \mathcal{O}\left(\frac{1}{\tilde{r}^4}\right) \quad (10b)$$

where  $h$  refers to the axion parameter. For the solution of the Kalb-Ramond field strength and the axion field one is referred to [41, 42]. Just like the JNW space time this metric also smoothly translates to the Schwarzschild solution in the event the axion parameter  $h$  vanishes.

We have already explored the properties of accretion and shadow in the spacetime with the axionic charge [43, 44]. In this work, we will explore the motion of both the massless and the massive particles around the Janis-Newman-Winicour spacetime. In case of massive particles we will study accretion of matter, while the properties of the black hole shadow can be investigated by studying motion of the massless particles. In both cases we will confront our theoretical findings with the available observations to provide constrain on the metric parameter  $\gamma$ . In each case we will compare our findings with the results obtained previously for the axion metric (Eq. (9), Eq. (10a), Eq. (10b)).

### 3 Shadow cast by the compact object governed by the Janis-Newman-Winicour spacetime

With the advent of the Event Horizon Telescope, it has been possible to obtain the image of the central compact object in the galaxy M87. This is complimentary to the electromagnetic observations related to accretion. The shadow refers to the gravitationally lensed projection of the photon circular orbits onto the observer's sky. When light from a distant source or the surrounding accretion disk come close to the photon sphere, a part of it falls into the compact object while the remaining escapes to infinity [45–49]. Consequently, the observer perceives a dark patch in the local sky known as the shadow. The boundary of the shadow testifies strong gravitational lensing near the photon sphere and hence the shape and size of the shadow captures useful information regarding the nature of the background spacetime [20, 47, 50–52]. In what follows, we will study the nature of the shadow cast by the Janis-Newman-Winicour spacetime and confront it with the observed shadow of M87\*. We initiate by first exploring the structure of the shadow in a most general spherically symmetric spacetime.

#### 3.1 Structure of the shadow in a general spherically symmetric background

In this section, we work out the structure of the black hole shadow in a general static and spherically symmetric background given by

$$ds^2 = -e^{\nu(r)} dt^2 + e^{\lambda(r)} dr^2 + \mathcal{R}^2(r) r^2 (d\theta^2 + \sin^2 \theta d\phi^2) \quad (11)$$

This metric ansatz is a more generalized form than the one usually used in the literature due to its modified volume factor, i.e. the coefficient of  $d\Omega^2$  is not just  $r^2$  but also has a function of  $r$  multiplied to it. This is important since we are eventually interested in studying the properties of the shadow in a metric given by Eq. (2).

Due to the time and zenithal angle independence of the metric, the energy  $E$  and the total angular momentum  $L$  of the photons are conserved. The constants of motion are given by,

$$E = -g_{tt}u^t = -p_t \quad \text{and} \quad (12a)$$

$$L = g_{\phi\phi}u^\phi = p_\phi \quad (12b)$$

respectively. The Hamilton-Jacobi equation can therefore be integrated to obtain the following solution for the action,

$$S = -Et + L\phi + \bar{S}(r, \theta) \quad (13)$$

where  $\bar{S}(r, \theta)$  is an arbitrary function of radial and angular coordinates. Assuming separability of  $\bar{S}(r, \theta)$  as  $\bar{S}(r, \theta) = S^r(r) + S^\theta(\theta)$ , and substituting the Hamilton-Jacobi equation for  $r$  and  $\theta$  in the Hamiltonian we obtain,

$$\mathcal{R}^2 r^2 \left( k + e^{-\nu(r)} E^2 - e^{-\lambda(r)} \left( \frac{dS^r}{dr} \right)^2 \right) = \left( \frac{dS^\theta}{d\theta} \right)^2 + \frac{L^2}{\sin^2 \theta} = C + L^2 \quad (12)$$

where the separation constant  $C$ , known as the Carter constant represents a third constant of motion [53]. Therefore the geodesic equations for  $r$  and  $\theta$  are given by,

$$e^{\lambda+\nu} \dot{r}^2 = -e^\nu \frac{C + L^2}{r^2 \mathcal{R}^2} + E^2 \equiv -V_{\text{eff}}(r) + E^2 \equiv \mathbf{R}(r) \quad \text{and} \quad (13)$$

$$\left( \mathcal{R}^2 r^2 \dot{\theta} \right)^2 = C - L^2 \cot^2 \theta \equiv E^2 \Theta(\theta) \quad (14)$$

respectively, where

$$V_{\text{eff}} = e^\nu \frac{C + L^2}{r^2 \mathcal{R}^2} \quad (15)$$

represents the effective potential for radial motion of photon, while

$$\Theta(\theta) = \chi - l^2 \cot^2 \theta \quad (16)$$

such that  $\chi = C/E^2$  and  $l = L/E$ . The radius of the photon sphere  $r_{ph}$  is defined such that the radial velocity  $\dot{r}$  vanishes and the effective potential  $V_{\text{eff}}(r)$  possesses an extrema. Generally this turns out to be a maxima, representing an unstable equilibrium of the photon, resulting in either fall into the gravitating object or escaping to infinity due to even slight perturbation. Consequently, photon sphere plays the important role in determining the boundary of the shadow.

Therefore,  $r_{ph}$  is obtained by solving  $\mathbf{R}(r) = \mathbf{R}'(r) = V'_{\text{eff}}(r) = 0$ , such that the above conditions yield

$$\chi + l^2 = \mathcal{R}^2(r_{ph}) r_{ph}^2 e^{-\nu(r_{ph})} \quad \text{and} \quad (17)$$

$$\nu'(r_{ph}) = 2 \left[ \frac{1}{r_{ph}} + \frac{\mathcal{R}'(r_{ph})}{\mathcal{R}(r_{ph})} \right] \quad (18)$$

respectively. The photon sphere in an arbitrary spherically symmetric metric is therefore obtained by solving Eq. (18) for  $r$ . In the limit  $\mathcal{R} = 1$  we get back the known result  $r\nu' = 2$  [44].

The contour of the black hole shadow in the observer's sky is obtained by considering the projection of the photon sphere in the image plane [54]. Determination of the shadow outline depends on the largest positive radius obtained by solving Eq. (18) [45, 46]. Two celestial coordinates  $\alpha$  and  $\beta$  which are directly related to  $l$  and  $\chi$  designates the locus of the shadow boundary [46, 54].

Following the prescription as given in [44, 46], it can be shown that

$$\alpha^2 + \beta^2 = \chi + l^2 = r_{sh}^2 \quad (19)$$

From the above analysis it can be concluded that for any general static, spherically symmetric and asymptotically flat metric the shadow is circular in shape and depends on the radius of photon sphere which in turn solely depends only on the  $g_{tt}$  component of the metric. We also note that for an asymptotically flat observer the radius of the shadow does not depend on the distance  $r_0$  and the inclination angle  $\theta_0$  of the observer.

### 3.2 Shadow of the compact object governed by the Janis-Newman-Winicour spacetime

In this section we will study the properties of the shadow given by the metric in Eq. (2). Before we proceed with the discussion of the shadow, we first plot the effective potential discussed in the last section in Fig. 1a. The figure depicts the behaviour of the effective potential with the variation of the metric parameter  $\gamma$ . As expected, the effective potential  $V_{eff}$  has a maxima occurring at the photon sphere  $r_{ph}$ , which depends on the value of  $\gamma$ . On decreasing the scalar charge  $q$  (or increasing  $\gamma$ ),  $r_{ph}$  becomes smaller along with the height of the potential.

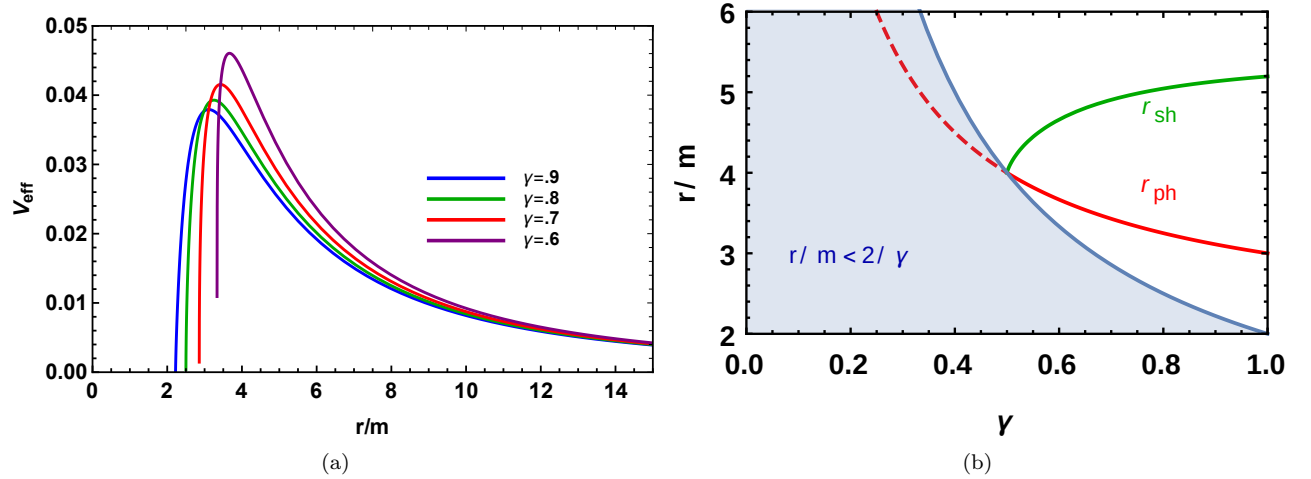


Figure 1: The above figure depicts the dependence of (a) the effective potential (b) photon sphere and the radius of the shadow on the metric parameter  $\gamma$ .

We can further determine the radius of the photon sphere and the shadow using Eq. (18) and Eq. (19) for the metric in Eq. (2). These are given by

$$\tilde{r}_{ph} = b \left( \gamma + \frac{1}{2} \right) \quad \text{and} \quad (20)$$

$$\tilde{r}_{sh} = b \left( \gamma + \frac{1}{2} \right) \left( \frac{2\gamma - 1}{2\gamma + 1} \right)^{\frac{1}{2} - \gamma} \quad (21)$$

respectively. From [Section 2](#) we recall that  $b\gamma = 2$  and  $0 \leq \gamma \leq 1$ . We note that as we decrease the value of  $\gamma$  from unity, the radius of the photon sphere  $r_{ph}$  increases while that of the shadow  $r_{sh}$  decreases. At  $\gamma = 0.5$  both  $r_{ph}$  and  $r_{sh}$  become equal to  $\tilde{r}_c = b$ , the radius where the curvature singularity occurs. When  $\gamma < 0.5$ ,  $r_{ph} < \tilde{r}_c$  and therefore we confine ourselves in the region  $0.5 \leq \gamma \leq 1$ . The above discussion is illustrated in [Fig. 1b](#). The region of unphysical solutions ( $\tilde{r} < b$ ) is shaded in blue. As soon as the field parameter  $\gamma$  approaches the critical value  $\gamma = 0.5$ , physical solutions for  $r_{ph}$  and  $r_{sh}$  ceases to exist.

At a glance, this atypical behaviour of photon sphere and shadow seems counter-intuitive since the radius of the shadow generally increases with the radius of the photon sphere. In this respect the behavior of the Winicour solution is quite unique. But one can understand this scenario with the analogy of having an optical lens system in a medium denser than air. Optical system in relatively denser medium bends light relatively smaller. Similarly, increasing the scalar charge  $q$  is equivalent to putting the optical system in a relatively denser medium i.e. a medium with larger refractive index. Consequently, light bending is maximum in the Schwarzschild scenario compared to the situation where there is scalar charge. The diagrammatic realisation has been shown in [Fig. 2](#) which clearly shows that the presence of scalar field causes lesser deflection of light compared to the Schwarzschild scenario.

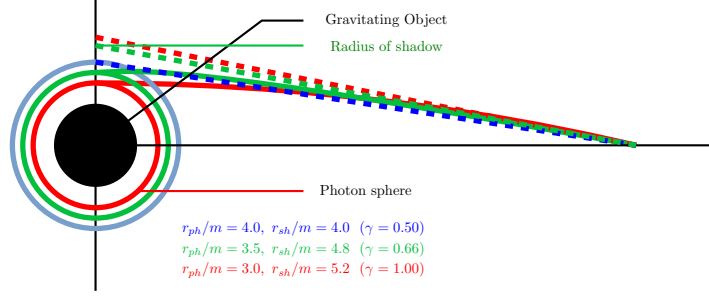


Figure 2: Diagrammatic realisation of gravitational lensing in Winicour spacetime

Finally we end our discussion with a few interesting comments:

- We have noted from [Section 2](#) that the scalar field and the Kalb-Ramond field both minimally coupled to gravity give rise to identical energy-momentum tensor. However, in the case of the scalar field the solution of the gravitational field equations lead to an exact metric representing a naked singularity while in the other case the solution leads to a perturbative metric representing a black hole. We have explored in an earlier work [\[44\]](#) the dependence of the shadow radius on the axion parameter  $h$  and found that a negative  $h$  enhances, while a positive  $h$  diminishes the shadow compared to the Schwarzschild scenario. In the Winicour solution on the other hand, the shadow decreases with decrease in  $\gamma$  (or increase with the scalar charge) and its radius is always less than the Schwarzschild case. This is illustrated in [Fig. 3](#).
- We note from [Fig. 3b](#) that the Schwarzschild scenario produces larger radius for the shadow compared to the ones with non-trivial scalar charge. This result has important implications with respect to the observed shadow of M87\*. It is known that the angular diameter of the shadow increases for an object with a larger shadow radius and bigger mass while decreases with the distance from the observer.

Recently, the Event Horizon Telescope Collaboration have released the image of the compact object M87\* in the centre of the galaxy M87 [55–60]. The angular diameter of the shadow is estimated to be  $42 \pm 3 \mu\text{as}$  and its mass is constrained to be  $M \sim 6.2_{-0.5}^{+1.1} \times 10^9 M_\odot$  [61] from stellar dynamics measurements while  $M \sim 3.5_{-0.3}^{+0.9} \times 10^9 M_\odot$  [62] from gas dynamics studies. Moreover, the distance of the source is reported to be  $D = (16.8 \pm 0.8) \text{ Mpc}$  [63–65] from stellar population measurements. The angle of inclination is taken to be  $17^\circ$  which the jet axis makes to the line of sight. Due to this small inclination angle the effect of angular momentum on the shape of the shadow gets suppressed. This also allows us to compare our spherically symmetric theory with the first image of the black hole.

From the above data, one can constrain the background spacetime created by the compact object M87\* through the radius of its shadow. We have shown earlier [44, 52] that given the mass and distance of M87\*, a spacetime which creates a shadow larger than the Schwarzschild scenario explains the observations better. In the current situation since the presence of the scalar field (smaller  $\gamma$ ) diminishes the shadow radius, the Schwarzschild scenario seems to be observationally more favored compared to the Winicour solution. However, it is important to note that while deriving the shadow radius we had implicitly assumed that the surrounding medium is optically thin such that the effect of the metric dominates the observed image. This may not be true and if the surrounding medium is optically thick then from the image of the surrounding accretion disk it is difficult to distinguish the JNW spacetime from the Schwarzschild metric [37].

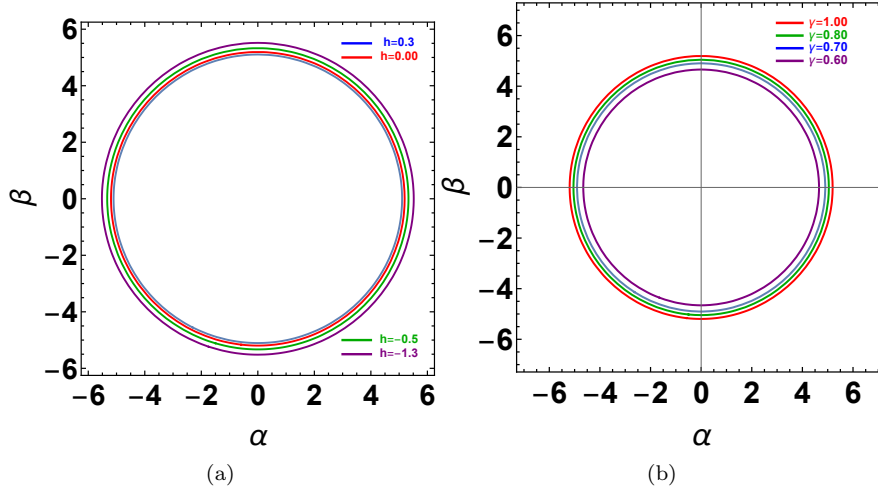


Figure 3: Radius of the shadow for (a) the perturbative axion metric and (b) the exact Winicour solution for various values of their respective metric parameters.

- We could have considered the metric ansatz in Eq. (2) by removing the constraint  $b\gamma = 2M$  and kept  $\gamma$  and  $b$  independent. Such a metric ansatz is compatible with the Einstein's equations with the minimally coupled scalar field. We refer to such a metric as the generalized Janis-Newman-Winicour solution. The interesting characteristic of this generalised solution is that we do not get physical solutions for the photon sphere and the shadow for all values of the metric parameters  $\gamma$  and  $b$ . In



Fig. 4, the regions  $b > 0, \gamma < 0$  and  $b < 0, \gamma > 0.5$ , produces negative radii for the photon sphere and the shadow and hence are not physically important. As discussed in Section 3.2 real positive solution of the shadow is achievable only if  $|\gamma| > 0.5$ . In fact for the region  $|\gamma| < 0.5$ , no physically realizable solution of photon sphere and shadow can be found (Fig. 1b). Hence the observation of shadow may be possible if  $b > 0, \gamma > 1/2$  or  $b < 0, \gamma < -1/2$ . The second scenario where  $b$  and  $\gamma$  are negative is not much discussed in the literature. However when we are in the region  $b > 0$  we must have  $\gamma b = 2$ , so that we can reproduce the Schwarzschild limit for the gravitating object. This particular case when  $b > 0$  is widely known as Janis-Newman-Winicour solution. Hence in this region, our two parameter solution reduces to one parameter solution discussed earlier. For the particular case when  $\gamma = 1$ , the solution in Eq. (2) represents the Schwarzschild solution.

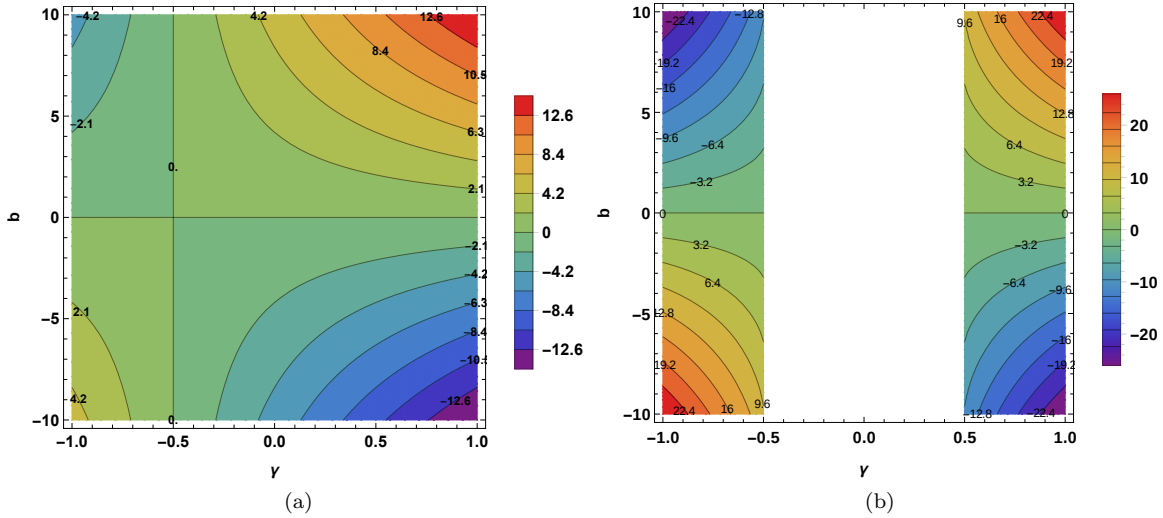


Figure 4: The above figure represents the constant contours of the radius of the (a) photon sphere and (b) the shadow as functions of the metric parameters  $\gamma$  and  $b$ . The shadow and the photon sphere are expressed in units of  $GM/c^2$ .

## 4 Accretion around the Janis-Newman-Winicour spacetime

In this section we investigate the properties of the electromagnetic emission from the accretion disk in the Janis-Newman-Winicour spacetime. The continuum spectrum emitted by the accretion disk depends not only on the nature of the background metric but also on the properties of the accretion flow. We assume the Novikov-Thorne model [66, 67] for the accretion disk where the disk is considered to be geometrically thin and optically thick. Accretion takes place chiefly along the equatorial plane such that the accreting particles have large azimuthal velocity  $v_\phi$  with negligible radial velocity  $v_r$  and even smaller vertical velocity  $v_z$ . The presence of viscosity in the system endows the accreting matter a small radial velocity which enables it to inspiral and fall into the central compact object. Within the domain of the Novikov-Thorne model the accreting matter has practically negligible  $v_z$  and hence the Novikov-Thorne accretion

disk harbors ‘no outflows’. As the accreting matter inspirals, they lose gravitational potential energy which gets converted into electromagnetic radiation. This radiation interacts very effectively with the accreting matter and almost all of it is radiated out from the system and no heat is trapped with the accretion flow. A temperature gradient exists within the disk such that the inner disk is much hotter compared to the outer disk. Since matter and radiation interacts very efficiently, every annulus of the disk emits a black body commensurate with the temperature of the disk. The integrated emission from the disk is therefore a multi-temperature black body radiation. With these assumptions of the ‘Novikov-Thorne’ model the flux from the accretion disk assumes an analytic form,

$$F = \frac{\dot{M}_0}{4\pi\sqrt{-g}}\tilde{f} \quad (22)$$

where,

$$\tilde{f} = -\frac{\Omega_{,r}}{(E - \Omega L)^2} \left[ EL - E_{ms}L_{ms} - 2 \int_{r_{ms}}^r LE_{,r'} dr' \right] \quad (23)$$

where,  $\Omega$ ,  $E$  and  $L$  are the angular velocity, specific energy and specific angular momentum of the accreting particle at the radial distance  $r$ . For a spherical symmetric metric, these can be expressed in terms of the metric parameters as,

$$\Omega = \frac{d\phi}{dt} = \frac{\sqrt{-\{g_{\phi\phi,r}\}\{g_{tt,r}\}}}{g_{\phi\phi,r}} \quad (24)$$

$$E = -u_t = \frac{-g_{tt}}{\sqrt{-g_{tt} - \Omega^2 g_{\phi\phi}}} \quad (25)$$

and

$$L = u_\phi = \frac{\Omega g_{\phi\phi}}{\sqrt{-g_{tt} - \Omega^2 g_{\phi\phi}}} \quad (26)$$

$E_{ms}$  and  $L_{ms}$  refer to the energy and angular momentum of the test particle at the marginally stable circular orbit. For a detailed discussion on the Novikov-Thorne model and a derivation of the expression for flux one is referred to [66–68].

Since the photon emits a Planck spectrum at every radius, the peak temperature is given by  $T(r) = \left(\tilde{F}(r)/\sigma\right)^{1/4}$  where  $\tilde{F}(r) = F(r)c^6/G^2$  with  $\sigma$  the Stefan Boltzmann constant. The luminosity from the thin accretion disk is obtained by integrating the Planck function  $B_\nu(T(r))$  over the disk surface at the observed frequency  $\nu$ , such that,

$$L_\nu = 8\pi^2 r_g^2 \cos i \int_{r_{ms}}^{r_{out}} \sqrt{-g} B_\nu(T(\tilde{r})) \tilde{r} d\tilde{r} \quad \text{and} \quad (27)$$

$$B_\nu(T) = \frac{2h\nu^3/c^2}{\exp\left(\frac{h\nu}{z_g kT}\right) - 1} \quad (28)$$

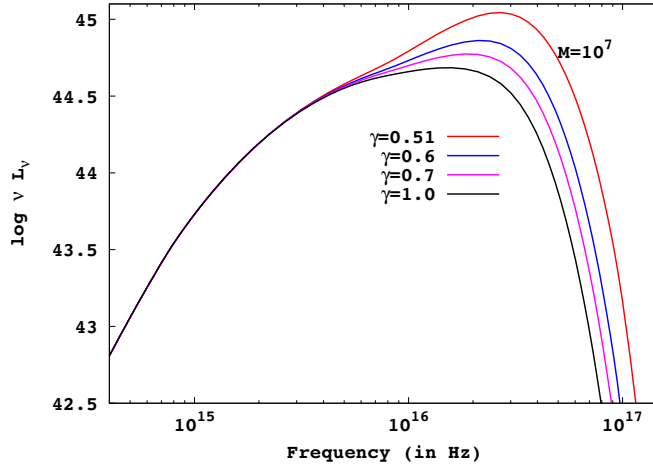


Figure 5: The above figure illustrates variation of the theoretically derived luminosity from the accretion disk with frequency for various values of  $\gamma$ . The background is given by Eq. (2). The luminosity decreases with increasing  $\gamma$  and is minimum in the general relativistic scenario where  $\gamma = 1$  (the Schwarzschild scenario). The representative mass of the black hole is taken to be  $M = 10^7 M_\odot$ . The accretion rate assumed is  $1 M_\odot \text{yr}^{-1}$  and  $\cos i$  is taken to be 0.8.

In Eq. (27),  $i$  refers to the inclination angle of the disk to the line of sight,  $r_g = GM/c^2$  denotes the gravitational radius, and  $z_g$  denotes the gravitational redshift factor given by,

$$z_g = E \frac{\sqrt{-g_{tt} - \Omega^2 g_{\phi\phi}}}{E - \Omega L} \quad (29)$$

The red-shift factor takes care of the modification induced in the photon frequency while travelling from the emitting material to the observer [69].

Note that the theoretical spectrum depends chiefly on the  $g_{tt}$  component of the metric while the  $g_{rr}$  component and the volume factor is required only through the determinant of the metric (see Eq. (22), Eq. (27)) [43].

The dependence of the theoretical spectrum from the accretion disk on the metric parameter  $\gamma$  is illustrated in Fig. 5. We note that the presence of the scalar charge enhances the luminosity from the accretion disk. In the next section we will estimate the observationally favored value of  $\gamma$  by comparing the theoretically calculated luminosity with the observed luminosity of eighty Palomar Green quasars.

#### 4.1 Observational sample

In this section, we compute the optical luminosity of a sample of eighty Palomar Green quasars [70, 71] and compare these with the corresponding observed values. We compute  $L_{opt} \equiv \nu L_\nu$  at the wavelength 4861Å [71]. We are interested in the theoretical estimates of the optical luminosity since for supermassive black holes, the luminosity from the accretion disk generally peaks in the optical part of the spectrum. The masses of these quasars have been estimated earlier [72–78] while the accretion rates are reported in [71]. Using observed data in the optical [79], UV [80], far-UV [81], and soft X-ray [82], the bolometric

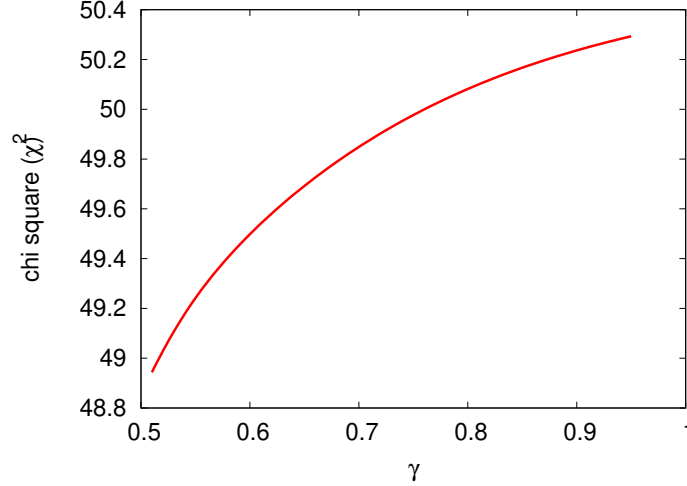


Figure 6: The above figure depicts  $\chi^2$  as a function of the metric parameter  $\gamma$ . It is evident from the plot that  $\chi^2$  minimizes for  $\gamma \sim 0.5$

luminosities of these quasars have been estimated. Since quasars have lower inclination angles we adopt  $\cos i \sim 0.8$  [71]. It turns out that for a Schwarzschild black hole the error (e.g., reduced  $\chi^2$ , Nash-Sutcliffe efficiency, index of agreement etc.) between the theoretical and observed luminosities get minimized when  $\cos i$  lies between  $0.77 - 0.82$  [83]. Moreover, Piotrovich et al. [84] estimated the inclination angles of some of the quasars in our sample which turns out to be consistent with our choice.

## 4.2 Numerical Analysis and error estimators

In this section we compute several error estimators which will enable us to deduce the observationally favored model of  $\gamma$ .

- **Chi-square  $\chi^2$**  : Consider a set of observed data  $\{\mathcal{O}_i\}$  with possible errors  $\{\sigma_i\}$ . The corresponding model estimates of the observed quantity is denoted by  $\Omega_i(\gamma)$ , where  $\gamma$  denotes the average scalar charge of the quasars. The  $\chi^2$  of the distribution is then given by,

$$\chi^2(\gamma) = \sum_i \frac{\{\mathcal{O}_i - \Omega_i(\gamma)\}^2}{\sigma_i^2} \quad (30)$$

For our sample, the error  $\{\sigma_i\}$  corresponding to optical luminosities of individual quasars are not reported. Hence we assign equal weightage to every observation. From Fig. 6 we note that  $\chi^2$  minimizes for  $\gamma \sim 0.5$  which implies that the Schwarzschild scenario with  $\gamma \sim 1.0$  is observationally less favored.

- **Nash-Sutcliffe Efficiency and its modified form:** Nash-Sutcliffe Efficiency  $E$  [85–87] is related to the sum of the squared differences between the observed and the predicted values normalized by

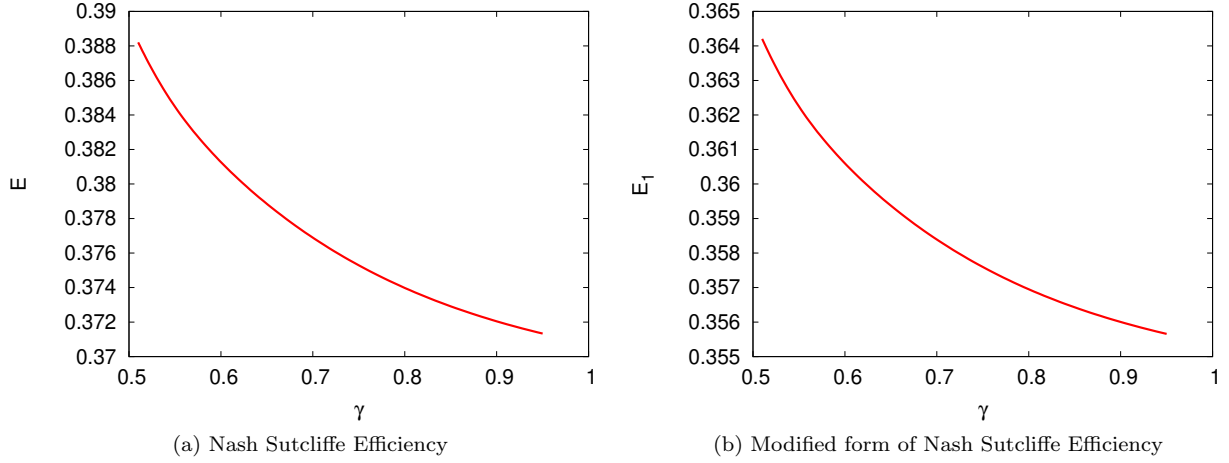


Figure 7: The above figure depicts variation of (a) the Nash-Sutcliffe Efficiency  $E$  and (b) the modified form of the Nash-Sutcliffe Efficiency  $E_1$  with the metric parameter  $\gamma$ . Both the error estimators maximize for  $\gamma \sim 0.5$ .

the variance of the observed values. This error estimator assumes the form,

$$E(\gamma) = 1 - \frac{\sum_i \{\mathcal{O}_i - \Omega_i(\gamma)\}^2}{\sum_i \{\mathcal{O}_i - \mathcal{O}_{av}\}^2} \quad (31)$$

where  $\mathcal{O}_{av}$  denotes average of the observed values of the optical luminosities of the quasars. Unlike  $\chi^2$ , the model which best describes the observation maximises the Nash-Sutcliffe Efficiency. A model with  $E \sim 1$  is considered to be an ideal model that accurately predicts the observations. As depicted in Fig. 7a in our case,  $E$  maximizes for  $\gamma \sim 0.5$ , indicating that such a model predicts the observation marginally better than the Schwarzschild scenario.

Nash-Sutcliffe Efficiency  $E$  tends to be oversensitive to higher values of the luminosity, for taking square of the error in the numerator (see e.g. Eq. (31)). Therefore, a modified version of the Nash-Sutcliffe Efficiency denoted by  $E_1$  [86] is used, where,

$$E_1(\gamma) = 1 - \frac{\sum_i |\mathcal{O}_i - \Omega_i(\gamma)|}{\sum_i |\mathcal{O}_i - \mathcal{O}_{av}|} \quad (32)$$

Similar to  $E$ , a model which maximizes  $E_1$  is considered to be a better description of the data. Fig. 7b illustrates that  $E_1$  maximizes for  $\gamma \sim 0.5$  and the conclusions drawn previously remain unaltered.

- **Index of agreement and its modified form:** The index of agreement was proposed [87–89] to overcome the insensitivity of the Nash-Sutcliffe Efficiency and its modified form towards the differences between the observed and predicted means and variances. Denoted by  $d$ , it assumes the form,

$$d(\gamma) = 1 - \frac{\sum_i \{\mathcal{O}_i - \Omega_i(\gamma)\}^2}{\sum_i \{|\mathcal{O}_i - \mathcal{O}_{av}| + |\Omega_i(\gamma) - \mathcal{O}_{av}|\}^2} \quad (33)$$

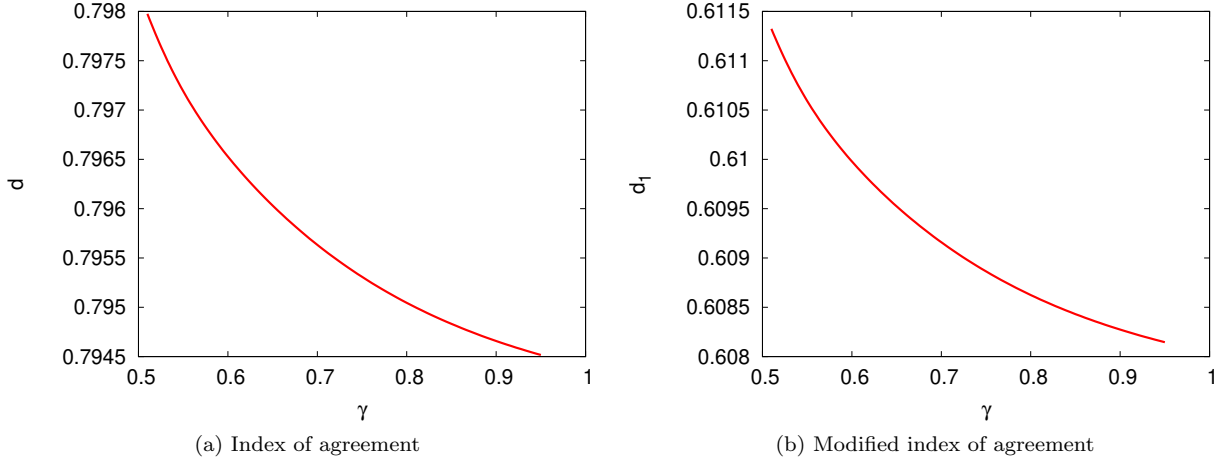


Figure 8: The above figure depicts variation of (a) index of agreement  $d$  and (b) the modified index of agreement  $d_1$  with the metric parameter  $\gamma$ . Both the error estimators maximize for  $\gamma \sim 0.5$ .

The denominator, which denotes the maximum deviation of each pair of observed and predicted luminosities from the average luminosity is known as the potential error.

Similar to Nash-Sutcliffe Efficiency, the index of agreement suffers from oversensitivity to higher values of optical luminosity and hence its modified version  $d_1$  is proposed, where,

$$d_1(\gamma) = 1 - \frac{\sum_i |\mathcal{O}_i - \Omega_i(\gamma)|}{\sum_i \{|\mathcal{O}_i - \mathcal{O}_{av}| + |\Omega_i(\gamma) - \mathcal{O}_{av}|\}} \quad (34)$$

Similar to the previous error estimators, we note from Fig. 8a and Fig. 8b that the model which best describes the observation maximizes  $d$  and  $d_1$  and hence corresponds to  $\gamma \sim 0.5$ . The Schwarzschild scenario is marginally disfavored.

## 5 Conclusion

The main goal of this work is to explore the characteristics of electromagnetic observations in the Janis-Newman-Winicour spacetime and confront them with the available observational data. This naturally involves investigating the nature of the black hole shadow and accretion in this background. Below we enlist the important results of this work:

- While investigating the properties of the shadow we note that the presence of the scalar charge decreases the effects of the gravitational lensing and diminishes the shadow radius compared to the Schwarzschild scenario. Since the observed shadow of M87\* exhibits an angular diameter greater than a Schwarzschild black hole, the JNW spacetime is even less favored from this observation. In a future observation if the angular diameter is found to be less compared to the Schwarzschild scenario, one can explore the possibility of JNW spacetime to explain the data.

- With the increase in scalar charge or decrease in  $\gamma$  the radius of the photon sphere increases while that of the shadow decreases. This feature is one of the unique properties of the Janis-Newman-Winicour spacetime.
- In the Winicour solution when the metric parameters  $\gamma$  and  $b$  are treated as independent, a new regime emerges where  $b$  is negative and  $\gamma \leq -0.5$ . This represents a horizonless compact object with real positive solutions for photon sphere and shadow. This is an interesting generalization in the parameter space of the Janis-Newman-Winicour spacetime which has not been discussed much in the literature.
- Apart from studying the nature of the shadow in the Janis-Newman-Winicour spacetime, we also explore the effects of this background on the accretion onto the compact object. We compute the theoretical luminosity from the accretion disk for a sample of eighty Palomar Green quasars and compare them with the corresponding observations. Several error estimators are computed to evaluate the observationally favored value of  $\gamma$  which reveals that an average  $\gamma \sim 0.5$  is the most favored model of scalar charge for the quasars.

Our error analysis reveals that accretion data clearly favours the presence of scalar charge. It is however important to mention that the quasars are multicomponent systems containing the accretion disk, the corona, the jet and the dusty torus emitting in all bands of the electromagnetic spectrum and we have modelled only the emission from the accretion disk. This is because modelling the entire spectral energy distribution (SED) theoretically is extremely challenging which is why one resorts to phenomenological models. Our goal in this work is not to model the entire SED but to constrain the value of  $\gamma$  from the accretion observations using a theoretical model for the disk. Amongst the available theoretical models the Novikov-Thorne model is very successful in modelling the emission from the accretion disk and our work is simply a first attempt to identify the observationally favored value of the scalar charge of the JNW spacetime from accretion data. While a more comprehensive theoretical modelling of the SED is necessary for a clearer understanding of the background metric we can clearly state at this point that modelling the emission from the accretion disk (optical/UV part of the spectrum) by the thin disk approximation favors the Janis-Newman-Winicour spacetime compared to the Schwarzschild scenario.

## References

- [1] P. S. Joshi and I. H. Dwivedi, “Naked singularities in spherically symmetric inhomogeneous Tolman-Bondi dust cloud collapse,” *Phys. Rev.* **D47** (1993) 5357–5369, [arXiv:gr-qc/9303037 \[gr-qc\]](#).
- [2] B. Waugh and K. Lake, “Strengths of Shell Focusing Singularities in Marginally Bound Collapsing Selfsimilar Tolman Space-times,” *Phys. Rev.* **D38** (1988) 1315–1316.
- [3] D. Christodoulou, “Violation of cosmic censorship in the gravitational collapse of a dust cloud,” *Commun. Math. Phys.* **93** (1984) 171–195.
- [4] D. M. Eardley and L. Smarr, “Time function in numerical relativity. Marginally bound dust collapse,” *Phys. Rev.* **D19** (1979) 2239–2259.
- [5] A. Ori and T. Piran, “Naked Singularities in Selfsimilar Spherical Gravitational Collapse,” *Phys. Rev. Lett.* **59** (1987) 2137.

- [6] R. Giambo, F. Giannoni, G. Magli, and P. Piccione, “Naked singularities in the gravitational collapse of barotropic spherical fluids,” *Gen. Rel. Grav.* **36** (2004) 1279–1298, [arXiv:gr-qc/0303043 \[gr-qc\]](#).
- [7] S. L. Shapiro and S. A. Teukolsky, “Formation of naked singularities: The violation of cosmic censorship,” *Phys. Rev. Lett.* **66** (1991) 994–997.
- [8] K. Lake, “Naked singularities in gravitational collapse which is not self-similar,” *Phys. Rev.* **D43** no. 4, (1991) 1416.
- [9] R. Goswami and P. S. Joshi, “Spherical gravitational collapse in N-dimensions,” *Phys. Rev.* **D76** (2007) 084026, [arXiv:gr-qc/0608136 \[gr-qc\]](#).
- [10] P. S. Joshi, N. Dadhich, and R. Maartens, “Why do naked singularities form in gravitational collapse?,” *Phys. Rev.* **D65** (2002) 101501, [arXiv:gr-qc/0109051 \[gr-qc\]](#).
- [11] T. Harada, H. Iguchi, and K.-i. Nakao, “Naked singularity formation in the collapse of a spherical cloud of counter rotating particles,” *Phys. Rev.* **D58** (1998) 041502, [arXiv:gr-qc/9805071 \[gr-qc\]](#).
- [12] R. Penrose, “Gravitational collapse: The role of general relativity,” *Riv. Nuovo Cim.* **1** (1969) 252–276. [Gen. Rel. Grav.34,1141(2002)].
- [13] Z. Kovacs and T. Harko, “Can accretion disk properties observationally distinguish black holes from naked singularities?,” *Phys. Rev.* **D82** (2010) 124047, [arXiv:1011.4127 \[gr-qc\]](#).
- [14] M. Blaschke and Z. Stuchlk, “Efficiency of the Keplerian accretion in braneworld Kerr-Newman spacetimes and mining instability of some naked singularity spacetimes,” *Phys. Rev.* **D94** no. 8, (2016) 086006, [arXiv:1610.07462 \[gr-qc\]](#).
- [15] Z. Stuchlik and J. Schee, “Appearance of Keplerian discs orbiting Kerr superspinars,” *Class. Quant. Grav.* **27** (2010) 215017, [arXiv:1101.3569 \[gr-qc\]](#).
- [16] C. Bambi, K. Freese, T. Harada, R. Takahashi, and N. Yoshida, “Accretion process onto super-spinning objects,” *Phys. Rev.* **D80** (2009) 104023, [arXiv:0910.1634 \[gr-qc\]](#).
- [17] P. S. Joshi, D. Malafarina, and R. Narayan, “Equilibrium configurations from gravitational collapse,” *Class. Quant. Grav.* **28** (2011) 235018, [arXiv:1106.5438 \[gr-qc\]](#).
- [18] D. Pugliese, H. Quevedo, and R. Ruffini, “Equatorial circular motion in Kerr spacetime,” *Phys. Rev.* **D84** (2011) 044030, [arXiv:1105.2959 \[gr-qc\]](#).
- [19] P. Pradhan and P. Majumdar, “Circular Orbits in Extremal Reissner Nordstrom Spacetimes,” *Phys. Lett.* **A375** (2011) 474–479, [arXiv:1001.0359 \[gr-qc\]](#).
- [20] K. Hioki and K.-i. Maeda, “Measurement of the Kerr Spin Parameter by Observation of a Compact Object’s Shadow,” *Phys. Rev.* **D80** (2009) 024042, [arXiv:0904.3575 \[astro-ph.HE\]](#).
- [21] L. Yang and Z. Li, “Shadow of a dressed black hole and determination of spin and viewing angle,” *Int. J. Mod. Phys.* **D25** no. 02, (2015) 1650026, [arXiv:1511.00086 \[astro-ph.HE\]](#).



- [22] R. Takahashi, “Shapes and positions of black hole shadows in accretion disks and spin parameters of black holes,” *J. Korean Phys. Soc.* **45** (2004) S1808–S1812, [arXiv:astro-ph/0405099](#) [[astro-ph](#)]. [*Astrophys. J.* 611,996(2004)].
- [23] G. N. Gyulchev and S. S. Yazadjiev, “Gravitational Lensing by Rotating Naked Singularities,” *Phys. Rev.* **D78** (2008) 083004, [arXiv:0806.3289](#) [[gr-qc](#)].
- [24] K. S. Virbhadra and G. F. R. Ellis, “Gravitational lensing by naked singularities,” *Phys. Rev.* **D65** (2002) 103004.
- [25] K. S. Virbhadra, D. Narasimha, and S. M. Chitre, “Role of the scalar field in gravitational lensing,” *Astron. Astrophys.* **337** (1998) 1–8, [arXiv:astro-ph/9801174](#) [[astro-ph](#)].
- [26] K. S. Virbhadra and C. R. Keeton, “Time delay and magnification centroid due to gravitational lensing by black holes and naked singularities,” *Phys. Rev.* **D77** (2008) 124014, [arXiv:0710.2333](#) [[gr-qc](#)].
- [27] M. Patil and P. S. Joshi, “High energy particle collisions in superspinning Kerr geometry,” *Phys. Rev.* **D84** (2011) 104001, [arXiv:1103.1083](#) [[gr-qc](#)].
- [28] R. Shaikh, “Shadows of rotating wormholes,” *Phys. Rev.* **D98** no. 2, (2018) 024044, [arXiv:1803.11422](#) [[gr-qc](#)].
- [29] P. V. P. Cunha, C. A. R. Herdeiro, and M. J. Rodriguez, “Does the black hole shadow probe the event horizon geometry?,” *Phys. Rev.* **D97** no. 8, (2018) 084020, [arXiv:1802.02675](#) [[gr-qc](#)].
- [30] G. Gyulchev, P. Nedkova, V. Tinchev, and S. Yazadjiev, “On the shadow of rotating traversable wormholes,” *Eur. Phys. J.* **C78** no. 7, (2018) 544, [arXiv:1805.11591](#) [[gr-qc](#)].
- [31] P. G. Nedkova, V. K. Tinchev, and S. S. Yazadjiev, “Shadow of a rotating traversable wormhole,” *Phys. Rev.* **D88** no. 12, (2013) 124019, [arXiv:1307.7647](#) [[gr-qc](#)].
- [32] A. I. Janis, E. T. Newman, and J. Winicour, “Reality of the Schwarzschild Singularity,” *Phys. Rev. Lett.* **20** (1968) 878–880.
- [33] I. Z. Fisher, “Scalar mesostatic field with regard for gravitational effects,” *Zh. Eksp. Teor. Fiz.* **18** (1948) 636–640, [arXiv:gr-qc/9911008](#) [[gr-qc](#)].
- [34] K. A. Bronnikov and A. V. Khodunov, “SCALAR FIELD AND GRAVITATIONAL INSTABILITY,” *Gen. Rel. Grav.* **11** (1979) 13–18.
- [35] M. Wyman, “Static Spherically Symmetric Scalar Fields in General Relativity,” *Phys. Rev.* **D24** (1981) 839–841.
- [36] K. S. Virbhadra, “Janis-Newman-Winicour and Wyman solutions are the same,” *Int. J. Mod. Phys.* **A12** (1997) 4831–4836, [arXiv:gr-qc/9701021](#) [[gr-qc](#)].
- [37] G. Gyulchev, P. Nedkova, T. Vetsov, and S. Yazadjiev, “Image of the Janis-Newman-Winicour naked singularity with a thin accretion disk,” *Phys. Rev.* **D100** no. 2, (2019) 024055, [arXiv:1905.05273](#) [[gr-qc](#)].

- [38] A. N. Chowdhury, M. Patil, D. Malafarina, and P. S. Joshi, “Circular geodesics and accretion disks in Janis-Newman-Winicour and Gamma metric,” *Phys. Rev.* **D85** (2012) 104031, [arXiv:1112.2522 \[gr-qc\]](#).
- [39] A. I. Janis, E. T. Newman, and J. Winicour, “Reality of the schwarzschild singularity,” *Phys. Rev. Lett.* **20** (Apr, 1968) 878–880. <https://link.aps.org/doi/10.1103/PhysRevLett.20.878>.
- [40] M. Wyman, “Static spherically symmetric scalar fields in general relativity,” *Phys. Rev. D* **24** (Aug, 1981) 839–841. <https://link.aps.org/doi/10.1103/PhysRevD.24.839>.
- [41] S. Kar, S. SenGupta, and S. Sur, “Static spherisymmetric solutions, gravitational lensing and perihelion precession in Einstein-Kalb-Ramond theory,” *Phys. Rev.* **D67** (2003) 044005, [arXiv:hep-th/0210176 \[hep-th\]](#).
- [42] S. Kar, P. Majumdar, S. SenGupta, and A. Sinha, “Does a Kalb-Ramond field make space-time optically active?,” *Eur. Phys. J.* **C23** (2002) 357–361, [arXiv:gr-qc/0006097 \[gr-qc\]](#).
- [43] I. Banerjee, B. Mandal, and S. SenGupta, “In quest of axionic hairs in quasars,” *JCAP* **1803** no. 03, (2018) 039, [arXiv:1712.09554 \[gr-qc\]](#).
- [44] I. Banerjee, S. Sau, and S. SenGupta, “Implications of axionic hair on shadow of M87\*,” [arXiv:1911.05385 \[gr-qc\]](#).
- [45] P. V. P. Cunha and C. A. R. Herdeiro, “Shadows and strong gravitational lensing: a brief review,” *Gen. Rel. Grav.* **50** no. 4, (2018) 42, [arXiv:1801.00860 \[gr-qc\]](#).
- [46] A. de Vries, “The apparent shape of a rotating charged black hole, closed photon orbits and the bifurcation setA4,” *Classical and Quantum Gravity* **17** no. 1, (Dec, 1999) 123–144. <https://doi.org/10.1088%2F0264-9381%2F17%2F1%2F309>.
- [47] S. E. Gralla, D. E. Holz, and R. M. Wald, “Black Hole Shadows, Photon Rings, and Lensing Rings,” *Phys. Rev.* **D100** no. 2, (2019) 024018, [arXiv:1906.00873 \[astro-ph.HE\]](#).
- [48] A. A. Abdujabbarov, L. Rezzolla, and B. J. Ahmedov, “A coordinate-independent characterization of a black hole shadow,” *Mon. Not. Roy. Astron. Soc.* **454** no. 3, (2015) 2423–2435, [arXiv:1503.09054 \[gr-qc\]](#).
- [49] A. Abdujabbarov, M. Amir, B. Ahmedov, and S. G. Ghosh, “Shadow of rotating regular black holes,” *Phys. Rev.* **D93** no. 10, (2016) 104004, [arXiv:1604.03809 \[gr-qc\]](#).
- [50] C. Bambi, K. Freese, S. Vagnozzi, and L. Visinelli, “Testing the rotational nature of the supermassive object M87\* from the circularity and size of its first image,” *Phys. Rev.* **D100** no. 4, (2019) 044057, [arXiv:1904.12983 \[gr-qc\]](#).
- [51] S. Vagnozzi and L. Visinelli, “Hunting for extra dimensions in the shadow of M87\*,” *Phys. Rev.* **D100** no. 2, (2019) 024020, [arXiv:1905.12421 \[gr-qc\]](#).
- [52] I. Banerjee, S. Chakraborty, and S. SenGupta, “Silhouette of M87\*: A New Window to Peek into the World of Hidden Dimensions,” *Phys. Rev.* **D101** no. 4, (2020) 041301, [arXiv:1909.09385 \[gr-qc\]](#).

- [53] B. Carter, “Global structure of the Kerr family of gravitational fields,” *Phys. Rev.* **174** (1968) 1559–1571.
- [54] J. M. Bardeen, “Timelike and null geodesics in the Kerr metric,” in *Proceedings, Ecole d’Et de Physique Thorique: Les Astres Occlus: Les Houches, France, August, 1972*, pp. 215–240. 1973.
- [55] **Event Horizon Telescope** Collaboration, K. Akiyama *et al.*, “First M87 Event Horizon Telescope Results. I. The Shadow of the Supermassive Black Hole,” *Astrophys. J.* **875** no. 1, (2019) L1.
- [56] **Event Horizon Telescope** Collaboration, K. Akiyama *et al.*, “First M87 Event Horizon Telescope Results. II. Array and Instrumentation,” *Astrophys. J.* **875** no. 1, (2019) L2, [arXiv:1906.11239 \[astro-ph.IM\]](#).
- [57] **Event Horizon Telescope** Collaboration, K. Akiyama *et al.*, “First M87 Event Horizon Telescope Results. III. Data Processing and Calibration,” *Astrophys. J.* **875** no. 1, (2019) L3, [arXiv:1906.11240 \[astro-ph.GA\]](#).
- [58] **Event Horizon Telescope** Collaboration, K. Akiyama *et al.*, “First M87 Event Horizon Telescope Results. IV. Imaging the Central Supermassive Black Hole,” *Astrophys. J.* **875** no. 1, (2019) L4, [arXiv:1906.11241 \[astro-ph.GA\]](#).
- [59] **Event Horizon Telescope** Collaboration, K. Akiyama *et al.*, “First M87 Event Horizon Telescope Results. V. Physical Origin of the Asymmetric Ring,” *Astrophys. J.* **875** no. 1, (2019) L5, [arXiv:1906.11242 \[astro-ph.GA\]](#).
- [60] **Event Horizon Telescope** Collaboration, K. Akiyama *et al.*, “First M87 Event Horizon Telescope Results. VI. The Shadow and Mass of the Central Black Hole,” *Astrophys. J.* **875** no. 1, (2019) L6.
- [61] K. Gebhardt, J. Adams, D. Richstone, T. R. Lauer, S. M. Faber, K. Gultekin, J. Murphy, and S. Tremaine, “The Black-Hole Mass in M87 from Gemini/NIFS Adaptive Optics Observations,” *Astrophys. J.* **729** (2011) 119, [arXiv:1101.1954 \[astro-ph.CO\]](#).
- [62] J. L. Walsh, A. J. Barth, L. C. Ho, and M. Sarzi, “The M87 Black Hole Mass from Gas-dynamical Models of Space Telescope Imaging Spectrograph Observations,” *Astrophys. J.* **770** (2013) 86, [arXiv:1304.7273 \[astro-ph.CO\]](#).
- [63] J. P. Blakeslee, A. Jordan, S. Mei, P. Cote, L. Ferrarese, L. Infante, E. W. Peng, J. L. Tonry, and M. J. West, “The ACS Fornax Cluster Survey. V. Measurement and Recalibration of Surface Brightness Fluctuations and a Precise Value of the Fornax–Virgo Relative Distance,” *Astrophys. J.* **694** (2009) 556–572, [arXiv:0901.1138 \[astro-ph.CO\]](#).
- [64] S. Bird, W. E. Harris, J. P. Blakeslee, and C. Flynn, “The Inner Halo of M87: A First Direct View of the Red-Giant Population,” *Astron. Astrophys.* **524** (2010) A71, [arXiv:1009.3202 \[astro-ph.GA\]](#).
- [65] M. Cantiello *et al.*, “A Precise Distance to the Host Galaxy of the Binary Neutron Star Merger GW170817 Using Surface Brightness Fluctuations,” *Astrophys. J.* **854** no. 2, (2018) L31, [arXiv:1801.06080 \[astro-ph.GA\]](#).
- [66] I. D. Novikov and K. S. Thorne, “Astrophysics of black holes,” in *Black Holes (Les Astres Occlus)*, C. Dewitt and B. S. Dewitt, eds., pp. 343–450. 1973.

- [67] D. N. Page and K. S. Thorne, “Disk-Accretion onto a Black Hole. Time-Averaged Structure of Accretion Disk,” *Astrophys. J.* **191** (1974) 499–506.
- [68] I. Banerjee, S. Chakraborty, and S. SenGupta, “Decoding signatures of extra dimensions and estimating spin of quasars from the continuum spectrum,” [arXiv:1905.08043 \[gr-qc\]](#).
- [69] D. Ayzenberg and N. Yunes, “Black Hole Continuum Spectra as a Test of General Relativity: Quadratic Gravity,” *Class. Quant. Grav.* **34** no. 11, (2017) 115003, [arXiv:1701.07003 \[gr-qc\]](#).
- [70] M. Schmidt and R. F. Green, “Quasar evolution derived from the Palomar bright quasar survey and other complete quasar surveys,” *Astrophys. J.* **269** (1983) 352.
- [71] S. W. Davis and A. Laor, “The Radiative Efficiency of Accretion Flows in Individual AGN,” *Astrophys. J.* **728** (2011) 98, [arXiv:1012.3213 \[astro-ph.CO\]](#).
- [72] S. Kaspi, P. S. Smith, H. Netzer, D. Maoz, B. T. Jannuzi, and U. Givon, “Reverberation measurements for 17 quasars and the size mass luminosity relations in active galactic nuclei,” *Astrophys. J.* **533** (2000) 631, [arXiv:astro-ph/9911476 \[astro-ph\]](#).
- [73] S. Kaspi, D. Maoz, H. Netzer, B. M. Peterson, M. Vestergaard, and B. T. Jannuzi, “The Relationship between luminosity and broad-line region size in active galactic nuclei,” *Astrophys. J.* **629** (2005) 61–71, [arXiv:astro-ph/0504484 \[astro-ph\]](#).
- [74] T. A. Boroson and R. F. Green, “The Emission - line properties of low - redshift quasi-stellar objects,” *Astrophys. J. Suppl.* **80** (1992) 109.
- [75] B. M. Peterson *et al.*, “Central masses and broad-line region sizes of active galactic nuclei. II. A Homogeneous analysis of a large reverberation-mapping database,” *Astrophys. J.* **613** (2004) 682–699, [arXiv:astro-ph/0407299 \[astro-ph\]](#).
- [76] L. Ferrarese and D. Merritt, “A Fundamental relation between supermassive black holes and their host galaxies,” *Astrophys. J.* **539** (2000) L9, [arXiv:astro-ph/0006053 \[astro-ph\]](#).
- [77] K. Gebhardt *et al.*, “A Relationship between nuclear black hole mass and galaxy velocity dispersion,” *Astrophys. J.* **539** (2000) L13, [arXiv:astro-ph/0006289 \[astro-ph\]](#).
- [78] S. Tremaine *et al.*, “The slope of the black hole mass versus velocity dispersion correlation,” *Astrophys. J.* **574** (2002) 740–753, [arXiv:astro-ph/0203468 \[astro-ph\]](#).
- [79] G. Neugebauer, R. F. Green, K. Matthews, M. Schmidt, B. T. Soifer, and J. Bennett, “Continuum energy distributions of quasars in the Palomar-Green Survey,” *Astrophys. J.* **63**.
- [80] A. Baskin and A. Laor, “What controls the C IV line profile in active galactic nuclei?,” *Mon. Not. Roy. Astron. Soc.* **356** (2005) 1029–1044, [arXiv:astro-ph/0409196 \[astro-ph\]](#).
- [81] J. E. Scott, G. A. Kriss, M. Brotherton, R. F. Green, J. Hutchings, J. M. Shull, and W. Zheng, “A Composite extreme ultraviolet QSO spectrum from FUSE,” *Astrophys. J.* **615** (2004) 135–149, [arXiv:astro-ph/0407203 \[astro-ph\]](#).
- [82] W. N. Brandt, A. Laor, and B. J. Wills, “On the Nature of soft x-ray weak quasistellar objects,” *Astrophys. J.* **528** (2000) 637–649, [arXiv:astro-ph/9908016 \[astro-ph\]](#).

- [83] I. Banerjee, S. Chakraborty, and S. SenGupta, “Excavating black hole continuum spectrum: Possible signatures of scalar hairs and of higher dimensions,” *Phys. Rev.* **D96** no. 8, (2017) 084035, [arXiv:1707.04494 \[gr-qc\]](#).
- [84] M. Y. Piotrovich, Y. N. Gnedin, T. M. Natsvlishvili, and S. D. Buliga, “Constraints on spin of a supermassive black hole in quasars with big blue bump,” *ApSS* **362** (Dec., 2017) 231, [arXiv:1711.07272](#).
- [85] J. Nash and J. Sutcliffe, “River flow forecasting through conceptual models part i a discussion of principles,” *Journal of Hydrology* **10** no. 3, (1970) 282 – 290.  
<http://www.sciencedirect.com/science/article/pii/0022169470902556>.
- [86] D. R. Legates and G. J. McCabe, “Evaluating the use of goodness-of-fit measures in hydrologic and hydroclimatic model validation,” *Water Resources Research* **35** no. 1, (1999) 233–241.  
<http://dx.doi.org/10.1029/1998WR900018>.
- [87] P. Krause, D. P. Boyle, and F. Bäse, “Comparison of different efficiency criteria for hydrological model assessment,” *Advances in Geosciences* **5** (Dec., 2005) 89–97.
- [88] C. J. Willmott, “On the evaluation of model performance in physical geography,” in *Spatial statistics and models*, pp. 443–460. Springer, 1984.
- [89] C. J. Willmott, “On the validation of models,” *Physical Geography* **2** no. 2, (1981) 184–194,  
<http://www.tandfonline.com/doi/pdf/10.1080/02723646.1981.10642213>.  
<http://www.tandfonline.com/doi/abs/10.1080/02723646.1981.10642213>.